Emulsion Templating: Unexpected Morphology of Monodisperse Macroporous Polymers

Lukas Koch[1], Sophia Botsch[1], Cosima Stubenrauch[*1,2]

[1] Institute of Physical Chemistry, University of Stuttgart, Pfaffenwaldring 55, 70569 Stuttgart, Germany

[2] Institute of Advanced Studies (USIAS), Université de Strasbourg, F-67000 France
*cosima.stubenrauch@ipc.uni-stuttgart.de, 0049 711 685-64470

Abstract

Hypothesis

We synthesised monodisperse macroporous polymers via polymerisation of water-in-monomer droplet emulsions and obtained non-spherical pores with layered pore walls. We hypothesise that this morphology is caused by surfactant diffusion and phase separation during polymerisation.

Experiments

We varied the surfactant mass fraction of the emulsions and polymerised the templates with a water-soluble initiator. From the resulting macroporous polymers we determined the shape of the pores and thickness of the layers via scanning election microscopy. The response of the monomer/surfactant mixture to polymerisation was studied by a ternary phase diagram that simulated polymerisation.

Findings

The emergence of non-spherical pores with layered pore walls is indeed caused by surfactant diffusion and phase separation. During polymerisation the surfactant molecules diffuse either to the water/monomer interface or deeper into the continuous monomer phase. The first process results in non-spherical pores, while the second process generates layered pore walls.

Keywords

Emulsion Templating – Macroporous Polymers – Phase Separation – Surfactant Diffusion – Microfluidics

1 Introduction

Polymerising the continuous phase of a monodisperse, FCC[1] (high internal phase emulsion) packed water-in-monomer HIPE (high internal phase emulsion, volume fraction of dispersed phase ≥ 74%) with a water-soluble initiator leads to a monodisperse, macroporous polymer with an intriguing morphology.[2] In SEM (scanning electron microscopy) analysis, the pore cross-sections of these materials are hexagons that are not interconnected with each other and the pore walls consist of three distinctive layers (see Figure 1). Note that the three-dimensional shape of the pores is similar to a rhombic dodecahedron.

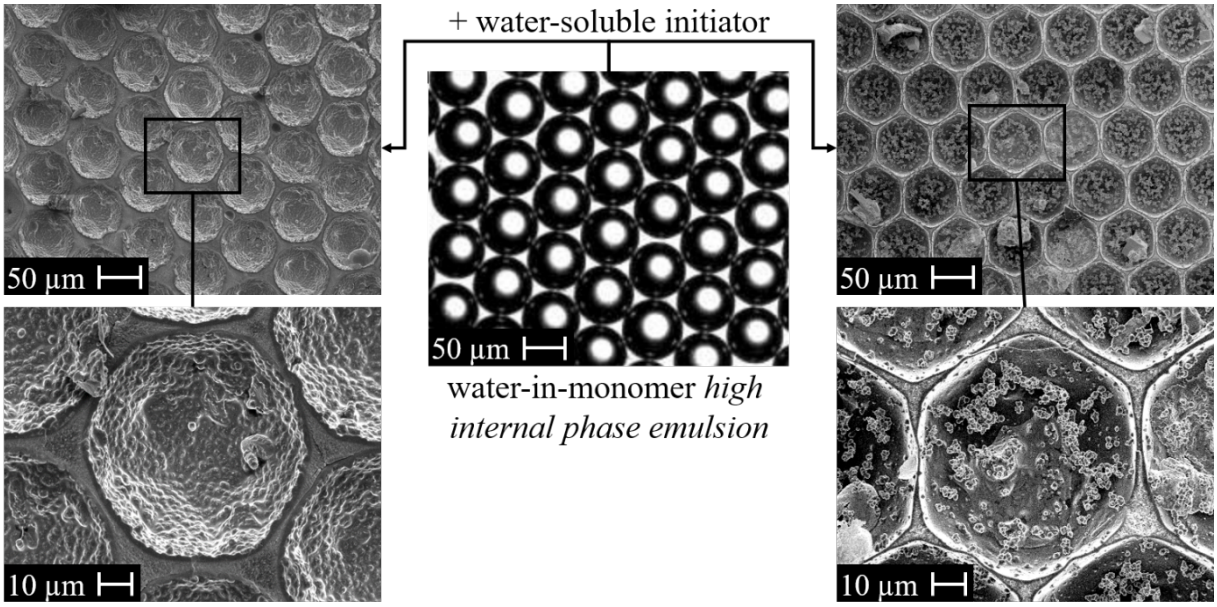

Figure 1: A monodisperse water-in-monomer *high internal phase emulsion* (middle) is polymerized with a water-soluble initiator leading to monodisperse, macroporous polystyrene/polydivinylbenzene (left) or monodisperse, macroporous poly-1,4-butanediol dimethacrylate (right).

This morphology was observed by both *Quell et al*. [1-4] (see Figure 1 (left)) and *Dabrowski et al*. [5] (see Figure 1 (right)) who used different monomers and surfactants. In their studies, they combined the concept of emulsion templating for styrene/DVB (divinylbenzene, cross-linker for styrene) [6-20] and for 1,4-BDDMA (1,4-butanediol dimethyacrylate) [21-23] with microfluidics [24-29]. *Quell et al*. [1-4] used a 50/50 mixture of styrene and DVB as monomers and the non-ionic, technical surfactant Hypermer 2296. *Dabrowski et al*. [5], on the other hand,

[1] FCC: face-centered cubic; HIPE: high internal phase emulsion; SEM: scanning electron microscopy; DVB: divinylbenzene; 1,4-BDDMA: 1,4-butanediol dimethyacrylate; KPS: potassium peroxydisulfate; AIBN: azobisisobutyronitrile; BPO: benzoyl peroxide; SEI: secondary electron imaging; SANS: small-angle neutron scattering

[2] The term "morphology" includes the shape, the size, the size distribution, and the interconnectivity of the pores as well as the thickness and texture of the pore walls.

used 1,4-BDDMA as monomer and the non-ionic, technical surfactant PGPR 4125. In both cases, KPS (potassium peroxydisulfate) was used as water-soluble initiator. When the monomer-soluble initiators AIBN (azobisisobutyronitrile) and BPO (benzoyl peroxide) were used instead, the pores were (a) spherical (like the initial water droplets) and (b) interconnected. In addition, the pore walls were porous. In order to end up with the shapes depicted in Figure 1 (left and right), the area of the water/monomer interface has to be increased during polymerisation since the surface area of a rhombic dodecahedron-shaped pore is roughly 10% larger than that of a spherical one if the volume is constant. Moreover, material has to be transported from the plateau borders (where three droplets meet) into the films (where two droplets meet) to obtain the thickness of the depicted pore walls. In the liquid state, the thickness of the films is only a few nanometers; however, it increases to values ranging from hundreds of nanometers to several micrometers in the polymerised state. In one of their publications, *Quell et al*. [3] proposed osmotic transport of DVB from the Plateau borders into the films driven by the depletion of the faster polymerising DVB [30] at the interface. They argued that osmotic transport of DVB is not only responsible for the structural change from spherical droplets to polyhedral pores, but also for the emergence of two outer (poly-DVB-rich) and one inner (polystyrene-rich) layer. However, this hypothesis cannot explain the results obtained by *Dabrowski et al*. [5], who used only one monomer, thus ruling out osmotic transport that depends on the presence of two monomers. Furthermore, the authors of the present study recently provided experimental evidence disproving osmotic transport [31]. In fact, in our study we showed that the development of the pore shape with varying styrene/DVB mass ratio or with KPS mass fraction was incompatible with the results that should have been obtained if osmotic transport was present and responsible for the morphological changes. In the present study, the shape of the pore cross-sections and the thickness of the layers in the pore wall were analysed quantitatively as function of the surfactant mass fraction in the HIPE templates. Moreover, the texture of the layers in the pore walls and the response of the surfactant to polymerization were investigated. Based on the results of these experiments, a new hypothesis was developed that explains why the interfacial area increases during polymerization and why three layers form in the pore walls.

2 Materials and Methods

Materials and Sample Preparation Styrene (99%), divinylbenzene (DVB, technical grade 80%, residual 20% is mostly ethylstyrene), polystyrene (average M_W = 35 000 g mol^{-1}),

potassium peroxydisulfate (KPS, 99%), and azobisisobutyronitrile (AIBN, 99%) were purchased from *Sigma-Aldrich*. The surfactant Hypermer 2296 was kindly provided by *Croda*. This technical surfactant primarily consists of polyisobutylene succinic anhydride sorbitan esters [32]. Deuterated Styrene (98%) was purchased from *Cambridge Isotopes*. D_2O (>99%) was purchased from *Eurisotop*. Double distilled water was used in all other experiments. All chemicals were used with further purification. The continuous monomer phase was prepared by dissolving the respective amount of Hypermer 2296 in a mixture of 5 g styrene and 5 g DVB. The surfactant mass fraction refers to the combined mass of monomers, thus the surfactant masses were between 0.5 g (5 wt.%) and 2.0 g (20 wt.%). The dispersed phase was 10 g H_2O. For polymerisation with a water-soluble initiator, the initiator mass fraction refers to the mass of H_2O. Thus, for an initiator mass fraction of 2.98 wt.%, 0.298 g KPS was dissolved in 10 g H_2O. For polymerisation with a monomer-soluble initiator, the initiator mass fraction refers to the combined mass of monomers. Thus, for an initiator mass fraction of 1.82 wt.%, 0.182 g AIBN was dissolved in 10 g monomers. Note that the initiator mass fractions of 2.98 wt.% KPS and 1.82 wt.% AIBN are equal in terms of molarity.

Preparation of Macroporous Polymers The samples were prepared as described in *Quell et al*. [1-4] and *Koch et al*. [31]. At first, the chemicals for the dispersed phase and the continuous monomer phase were weighed and blended in a 100 mL screw top DURAN® glass from *Schott*, respectively. Next, the two phases were connected to the microfluidic chip and to the pressure controller *OB I MkII* from *Elveflow* which controlled the flow rates via the software *Elveflow SI* from *Elveflow*. The microfluidic chip was purchased from *Dolomite* and had flow-focusing geometry, hydrophobic coating, and a constriction size of 100 x 105 µm. The generation of the water-in-monomer emulsions inside the chip were monitored with a *Nikon SMZ – 800 N* optical microscope coupled to an *Optronis CL600X2* high speed camera. The same device combined with the image processing program *ImageJ* was used to determine the size of the water droplets. After its generation, the emulsion was collected and the droplets were given time to sediment. After sedimentation was complete and a *high internal phase emulsion* (HIPE) had formed, the excess continuous monomer phase was removed and the samples were put into an oil bath at 70 °C for 24 hours (initiator AIBN) or 48 hours (initiator KPS). The final steps were the purification of the samples via Soxhlet extraction with ethanol for 12 hours and drying at 60 °C in a drying oven for 72 hours.

Analysis of Macroporous Polymers To facilitate the cutting of the macroporous polymers with a scalpel, they were cooled with liquid nitrogen. The direction of each cut was

positioned such that a layer of pores could be studied. A piece of roughly 5 x 5 x 2 mm was prepared and glued onto an *Aluminium Specimen Stub* from *Agar Scientific*. Next, the samples were put under vacuum and sputtered with a thin layer of gold. For the quantitative analysis of the pore cross-sections and the thickness of the layers in the pore walls, a *CamScan CS44* SEM ("SEM1") with SEI (secondary electron imaging) was used. The circumference C and area A of a pore cross-section was calculated by *ImageJ* after the pore cross-section had been encircled manually at a 100-fold magnification. The average number of encircled pore cross-sections was 62. The areas of the pore wall t, of the outer layer o, and of the inner layer were also calculated by *ImageJ*. Here, the respective shape of the areas was likewise traced manually for one strut. 500-fold magnifications were used and an average of 8 struts per sample were examined. An exemplary picture for one strut is provided in Figure 4 (left). Microscopic pictures at other magnifications were also taken. For the qualitative analysis of the texture of the pore walls and their layers, a Zeiss GeminiSEM 500 SEM ("SEM2") with SEI was used.

Phase Diagram For recording the surfactant – styrene – polystyrene phase diagram, mixtures of surfactant and styrene were prepared. The majority of each mixture was placed into a glass tube that was weighed before and after its filling. The glass tube was then tempered inside a water tank at 70 °C to mimic the temperature of the polymerization. Next, small polystyrene pellets were added to the mixtures to simulate the polymerization. When no more polystyrene could be dissolved and the mixture had undergone phase separation, the glass tube was weighed again to determine how much polystyrene had been added. Next, droplets of the initial surfactant/styrene mixture were added in order to return to the monophasic region and to thereby determine the position of the phase border more accurately.

Small angle neutron scattering The SANS (small-angle neutron scattering) measurements were conducted at the KWS-1 spectrometer at the Heinz Maier-Leibnitz Zentrum (MLZ) in Munich, Germany. Before measurement, deuterated styrene with 10 wt.% of surfactant was carefully placed over D_2O in order to bring the two phases into contact. A small fraction of the monomer phase was removed and put into a cuvette that was then placed into the SANS device. A neutron wavelength of 4.93 Å was used. The scattering intensity was measured from $q = 0.00978$ Å^{-1} to $q = 0.669$ Å^{-1} which required collimation/detector distances of 8 m / 8 m and 8 m / 1.5 m. The scattering intensity was normalized to an absolute scale via the incoherent scattering of the references H_2O and Perspex. Raw data treatment, masking and radial averaging to obtain a one-dimensional scattering curve were performed with the evaluation software QtiKWS.

Spinning Drop Tensiometer The Spinning Drop Video Tensiometer *SVT 15* by *DataPhysics Instruments* was used to determine the interfacial tension between H_2O and the surfactant/monomer mixtures at different temperatures. Roughly 100 µL of the surfactant/monomer mixture was added to a capillary filled with H_2O such that a droplet formed. The interfacial tension was determined by the software of the tensiometer with *LaPlace Young Fitting* by recording the shape of the droplet. Measurements were conducted at temperatures between 25 °C and 70 °C in steps of 15 °C and at spinning rates between 3000 rpm and 13000 rpm in steps of 2000 rpm. To enable *LaPlace Young Fitting* for the software, the density of the surfactant/monomer mixtures had to been known. This was achieved by measuring the density of the surfactant/monomer mixtures at the studied temperatures with the Density Meter *DMA 5000 M* by *Anton Paar*.

3 Results

The overall objective of our study was to find a mechanism that explains why and how the morphology depicted in Figure 1 is created. Since we had already varied the monomer mass ratio and initiator mass fraction in our previous study [31], the only component left to investigate was the surfactant mass fraction. A variation of this parameter could finally reveal the sought-after mechanism and therefore, surfactant mass fractions of 5, 10, 15, and 20 wt.% were used in this study. The styrene/DVB mass ratio was kept constant at 50/50 and the KPS mass fraction was also kept constant at 2.98 wt.%. In their original samples, *Quell et al*. [1-4] used this composition and a surfactant mass fraction of 10 wt.%. Figure 2 depicts the two-dimensional pore cross-sections of the four samples that were produced, collected, polymerised, purified, dried, and prepared for analysis in the manner described in Section 2. The pictures in the right row of Figure 2 were taken with a SEM ("SEM2" in Section 2) which is different from the one used for the left and middle rows ("SEM1"). With "SEM 2", pictures with higher magnifications can be taken. In this way, we were able to determine the texture of the layers in the pore walls.

3.1 Non-Spherical Pores

Looking at the left row of Figure 2, one sees that the shape of the pore cross-sections is hexagonal regardless of the respective surfactant mass fraction. This is not only true for the small excerpts shown in Figure 2 (left row), but also for the whole samples. As introduced in

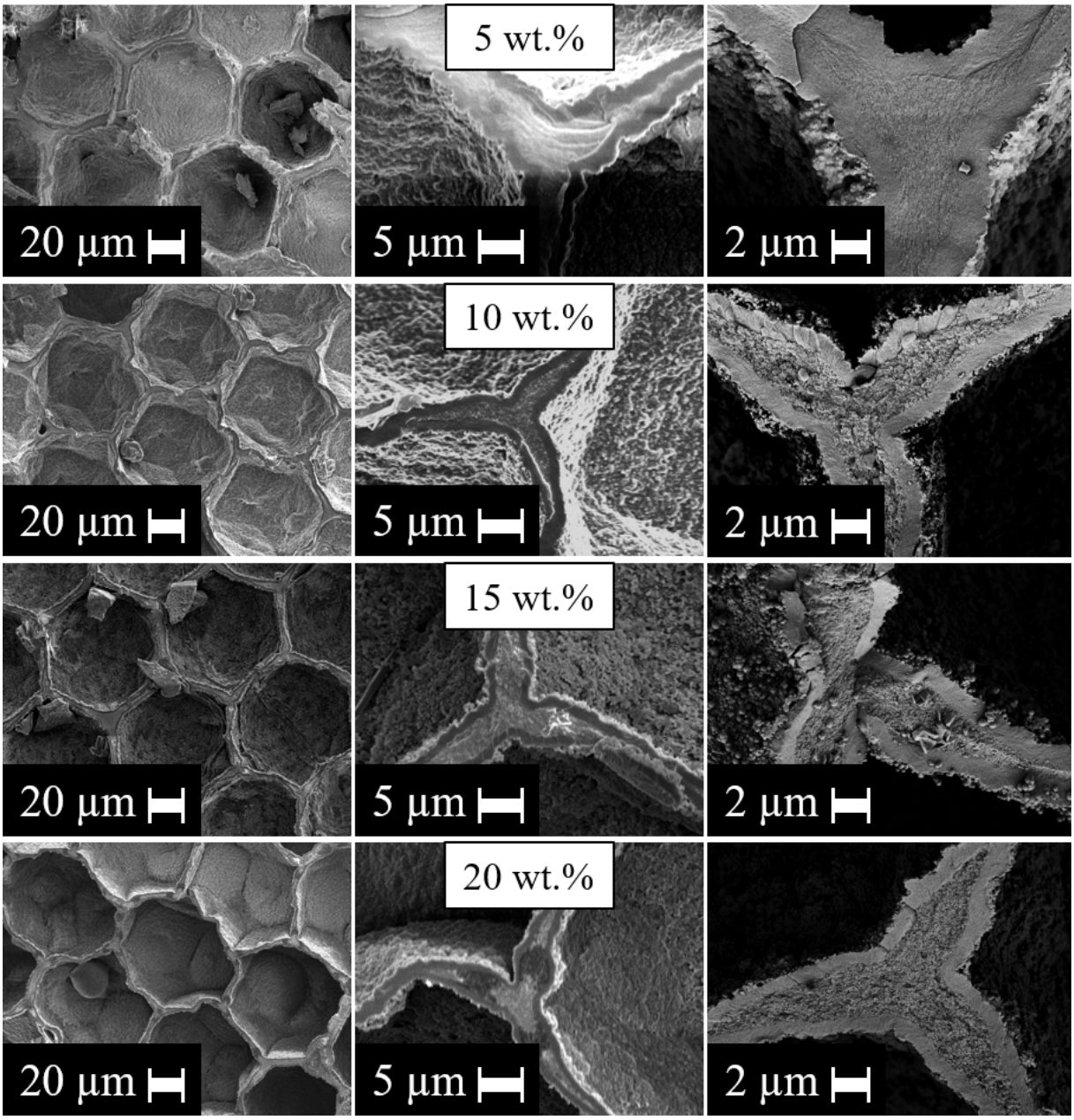

Figure 2: SEM pictures of macroporous polystyrene/poly-DVB obtained via polymerisation of monodisperse styrene/DVB HIPEs with a KPS mass fraction of 2.98 wt.%, a styrene/DVB mass ratio of 50/50, and surfactant mass fractions of 5, 10, 15, and 20 wt.%.

our previous publication [31], we used a so-called "shape-factor *S*" to describe the shape of the pore cross-sections in a quantitative way. The idea of using an actual number to describe shapes stems from foam science where something analogous is done in three dimensions [33-37]. We argued that even if *S* only takes into account the two-dimensional pore cross-sections, it serves as a sufficient indication for the three-dimensional shape of the pores that are not accessiblewith scanning electron microscopy. *S* is given as

$$S = \frac{1}{2 \cdot \sqrt{\pi}} \cdot \frac{C}{\sqrt{A}} \tag{1}$$

where C is the circumference and A is the area of a pore cross-section. The ratio between C and A is a measure for the shape of a pore cross-section since the ratio is smaller for more circular shapes and larger for more angular shapes. C and A are determined in the manner described in the Section 2. The square root of A is taken to make sure that S is independent of the size of the pores since C scales linearly and A scales quadratically with size. With the pre-factor $1/2\sqrt{\pi}$, one obtains $S = 1$ for circular shapes (see Figure 3 (bottom left)) and $S = 1.05$ for a hexagon (see Figure 3 (middle left)). For hexagonal pore cross-sections of real samples, S can be larger than 1.05 because the edges of the pore cross-sections are not necessarily straight lines, but can be "crumpled" (see Figure 3 (top left)). Hence, C is slightly larger, while A roughly stays the same and thus $S > 1.05$. Figure 3 (right) depicts the development of S as function of the surfactant mass fraction.

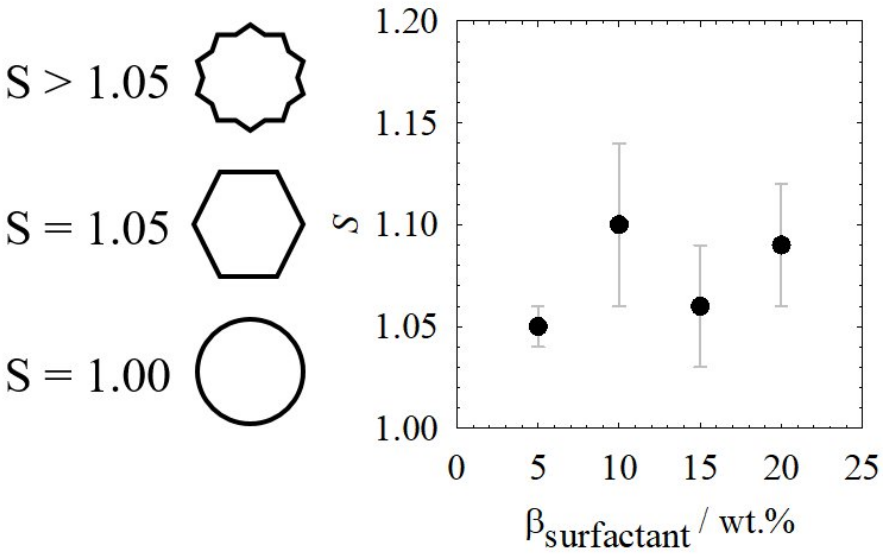

Figure 3: (left) Exemplary values of the shape-factor S for different shapes. (right) Shape-factor S as function of the surfactant mass fraction for a KPS mass fraction of 2.98 wt.% and a styrene/DVB mass ratio of 50/50.

Figure 3 (right) shows that the shape of the pore cross-sections is hexagonal for all samples since all values of S are 1.05 or slightly higher. As a reminder, the area of the water/monomer interface has to increase during polymerisation to end up with hexagonal pore cross-sections (rhombic dodecahedron-shaped pores). Apparently, this happens independently of the surfactant mass fraction. When monomer-soluble AIBN is used as initiator instead, the shape

of the pore cross-sections is always circular (see Figure SI-1) and also does not change with the surfactant mass fraction.

3.2 Layered Pore Walls

Figure 2 (middle row) depicts the development of the pore walls and their layers when the surfactant mass fraction is varied. At a first glance, one sees that both the overall thickness of the pore walls as well as the thickness of the layers are not constant. Since one of the reasons for this study was to find an explanation for the formation of the three layers in the pore walls, their thicknesses were measured. However, rather than going for the layer thicknesses, we opted to measure the layer areas. An example of how the layer areas were measured in one strut is given in Figure 4 (left).

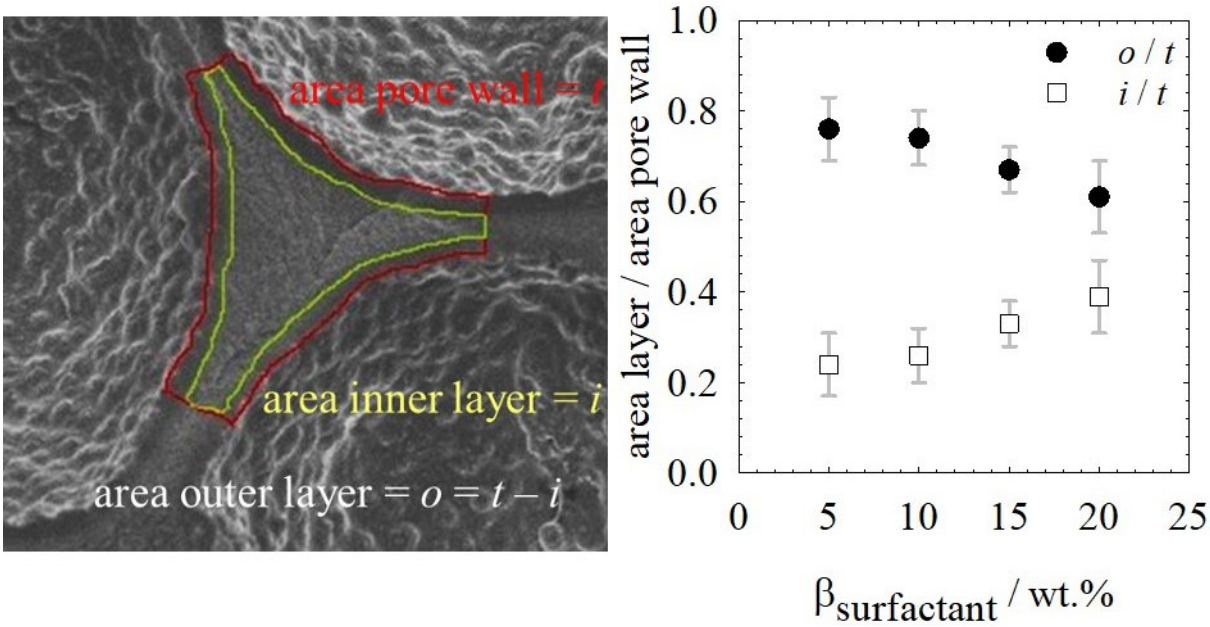

Figure 4: (left) Area determination of the total pore wall *t* (enclosed by red profile), of the inner layer *i* (enclosed by yellow profile), and of the outer layer *o* (calculated from the difference between *t* and *i*) in one strut. (right) Ratio *o* / *t* (black circles) and ratio *i* / *t* (white squares) as function of the surfactant mass fraction for a KPS mass fraction of 2.98 wt.% and a styrene/DVB mass ratio of 50/50.

The layer areas instead of the layer thicknesses were measured because the thickness of the inner layer changes significantly with the position where it is measured. While in the middle of a strut the thickness of the inner layer is rather large, it becomes increasingly smaller towards the borders of a strut (see Figure 4 (left)). Thus, it is difficult to find a reasonable value for the layer thickness. By taking the overall area of the layers instead, one gets rid of this problem

since all positions are taken into account. We also did not simply use the absolute layer areas, but the relative layer areas *o*/*t* (outer/total) and *i*/*t* (inner/total). Using only absolute areas, it is impossible to distinguish whether the area of a layer is changing (a) due to the variation of the surfactant mass fraction or (b) because the total area of the pore wall is changing. Regarding the magnifications of the SEM pictures, a compromise had to be found between lower magnifications where more struts can be measured and higher magnifications where it was possible to accurately determine the areas of the pore walls and of the layers. This compromise was found at a 500-fold magnification with an average number of 8 measured struts. Figure 4 (right) shows the development of the relative outer layer area *o*/*t* and of the relative inner layer area *i*/*t* as function of the surfactant mass fraction. It is clearly visible that the relative outer layer area *o*/*t* decreases and the relative inner layer area *i*/*t* increases when the surfactant mass fraction is increased. This suggests that the thickness and creation of the inner layer is linked to the surfactant mass fraction as will be discussed further below.

3.3 Porosity of the Inner Layer

In Figure 2 (right row), the texture of the layers becomes visible, i.e. the outer layers are compact and non-porous, while the inner layers seem to be porous. A porosity is caused when material is removed during purification and drying of the already polymerised samples. Knowing from the previous paragraph that the relative area of the inner layer increases when the surfactant mass fraction is increased, we reason that the porosity of the inner layer is caused by the surfactant. However, this still does not explain why surfactant molecules are only present in the inner and in the outer layers after polymerisation. Since the surfactant molecules are distributed evenly across the continuous monomer phase before polymerisation starts, they have to diffuse to the inner layers during polymerisation. To find out the driving force for surfactant diffusion, we simulated the polymerisation with a ternary phase diagram containing styrene, surfactant, and polystyrene at 70 °C by dissolving polystyrene in surfactant/styrene mixtures with different surfactant mass fractions. Note that DVB was not used in this model system since we found no purchasable poly-DVB with a defined molar mass. Further note that we excluded H_2O from the system to simplify the measurements. The ternary phase diagram containing surfactant, polystyrene, styrene at 70 °C is depicted in Figure 5. We found that adding polystyrene to the surfactant/styrene mixtures eventually leads to a phase separation (see Figure 5 (black dots)). However, the amount of polystyrene that can be added before phase separation occurs strongly depends on the surfactant mass fraction. When the surfactant mass fraction is

low, relatively high amounts of polystyrene can be added before the mixture turns biphasic (see Figure 5 (dashed arrow)). On the other hand, when the surfactant mass fraction is high, phase separation occurs at much lower amounts of added polystyrene (see Figure 5 (dotted arrow)). In other words, the surfactant does not "like" the polymerisation and wants to remain solubilised in the monomer.

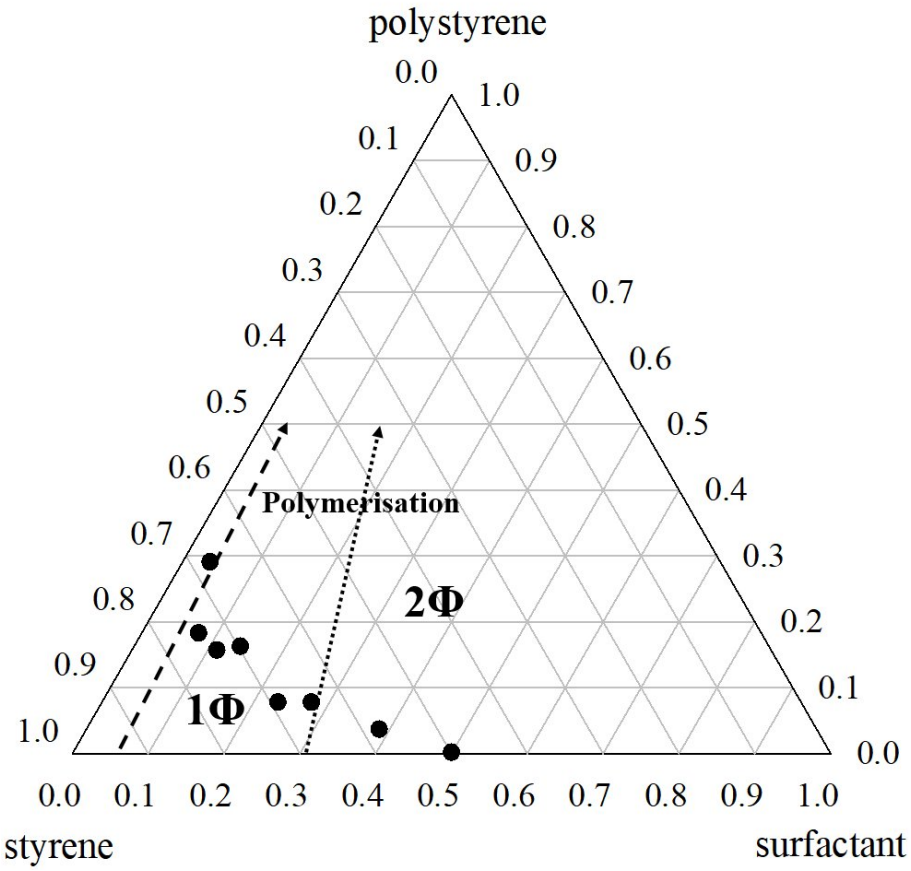

Figure 5: Model ternary phase diagram of the monomer styrene, the surfactant Hypermer 2296, and the polymer polystyrene at 70 °C. The black dots mark the positions of the measured phase boundaries. The arrows indicate the direction of the simulated polymerisation.

4 Discussion

After presenting the experimental data in the previous Section, we will now discuss what the results imply for the samples before, during, and after polymerisation. Based on these implications, in turn, we develop a hypothesis for a mechanism that explains why the interfacial area of the pores increases during polymerisation and why pore walls with three layers form. Figure 2 (left row) and Figure 3 in Section 3.1 revealed that the shape of the pore cross-sections is hexagonal independent of the surfactant mass fraction. Therefore, the mechanism that increases the area of the water/monomer interface during polymerisation is present in all

samples. Figure 2 (middle row) and Figure 4 (right) in Section 3.2 revealed that when the surfactant mass fraction is increased, the relative area of the outer layer decreases and the relative area of the inner layer increases. Therefore, we conclude that the formation of the inner layer is linked to the surfactant. In Figure 2 (right row), the texture of the layers became visible. While the outer layers are compact and non-porous, the inner layer is porous. Combined with the results from Section 3.2, we conclude that the surfactant is responsible for the porosity of the inner layer. For this to happen, surfactant molecules have to accumulate in the inner layer during polymerisation before they are washed out during purification. In turn, this also means that no significant amount of surfactant molecules is located in the outer layers since they are non-porous.

Firstly, we have to ask the question how much surfactant is required to stabilise the water/monomer interface. Based on this value, one can calculate how much surfactant is dissolved in the continuous monomer phase and is thus able to be present in the inner layer. Note that the surfactant Hypermer 2296 is not water-soluble. First, we calculated how high the surfactant mass fraction has to be to cover the whole interfacial area. This value depends on the droplet size and on the head group area one surfactant molecule covers at the water/monomer interface. The calculations are described for three droplet sizes in the Supporting Information (see Figure SI-2). For water droplets with a diameter of 80 µm and a surfactant molar mass of 833 g mol^{-1} [32], the necessary surfactant mass fraction is between 0.06 wt.% and 0.01 wt.% if one assumes head group areas between 50 $Å^2$ and 250 $Å^2$. Thus, even for the lowest surfactant mass fraction used in this study (5 wt.%), the overwhelming majority of surfactant molecules is dissolved in the continuous monomer phase and not located at the water/monomer interface.

Secondly, we also have to discuss whether the surfactant is solely responsible for the porosity of the inner layer or if other components also add to the porosity. To answer this question, we prepared the monomer phases (styrene, DVB, and surfactant) of the four samples and brought them into contact with water without mixing the two phases. We observed that the initially clear monomer phases became turbid (see Figure SI-3 in the Supporting Information). This indicates that structures able to scatter light are formed in the monomer phases. Without surfactant in the monomer phase or without bringing the surfactant-containing monomer phases into contact with water, no turbidity arose in the monomer phases. Thus, we conclude that the structures must consist of both surfactant and water. Since no additional energy was brought into the system by mixing, these structures formed spontaneously, i.e. the surfactant dissolved in the continuous monomer phase takes up small amounts of water from the dispersed phase. Note

that the interfacial tension between water and the monomer phases ranges between 0.5 mN m^{-1} and 1.0 mN m^{-1} for a temperature range of 25 °C and 70 °C. To determine the size of these structures, deuterated styrene with 10 wt.% surfactant was measured with SANS 8 minutes after it was brought into contact with deuterated water. When fitting the data with a Gaussian shell model [38], it was possible to identify the structures as vesicles with an average diameter of 11 ± 5 nm. The bilayer of the vesicles mainly consists of surfactant molecules with very small amounts of water located between the surfactant head groups. The SANS data as well as the fitted curve are shown in Figure SI-4 in the Supporting Information. To conclude, the observed porosity in the inner layers of the pore walls in Figure 2 (right row) mainly stems from the surfactant with small amounts of water adding to the porosity. With Figure 5 in Section 3.3, we demonstrate why the surfactant is depleted from the outer layers and accumulated in the inner layers. The amount of polystyrene that was added to the surfactant/styrene mixtures before phase separation was strongly dependent on the surfactant mass fraction. When increasing the surfactant mass fraction, phase separation happens at lower amounts of polystyrene. We therefore conclude that when the surfactant is exposed to the growing polymer, it diffuses away towards regions where no polymerisation is happening. Thereby, the surfactant can remain solubilised.

By combining all results from the two previous paragraphs, we are able to devise a hypothesis for a mechanism that explains both why the area of the water/monomer interface increases during polymerisation and why three layers form in the pore walls. A schematic drawing of this mechanism is presented in Figure 6. Note that for the sake of clarity, we left out the vesicles from the drawing and only show the surfactant molecules since they are the key players. Further note that the sizes of the surfactant molecules (red tail and blue head), of the water droplets (light blue), and of the space of the continuous monomer phase (orange) are not to scale. Before polymerisation, the water droplets inside the HIPE are spherical (circular in 2D schematical drawing of Figure 6) and the surfactant is either stabilising the water/monomer interface or being distributed homogeneously across the continuous monomer phase (see Figure 6 (a)). Once polymerisation is started at the water/monomer interface by the water-soluble initiator, a polystyrene/poly-DVB network (light brown) starts to form close to the water/monomer interface (see Figure 6 (b)). At this point in time, the majority of monomer molecules are still unpolymerised and thus, the region of the continuous monomer phase close to the water/monomer interface is still liquid. However, the beginning of the polymerisation causes a diffusion of surfactant molecules away from the polymerisation “zone”. The surfactant molecules have two directions where they can diffuse to (see Figure 6 (a and b, black arrows).

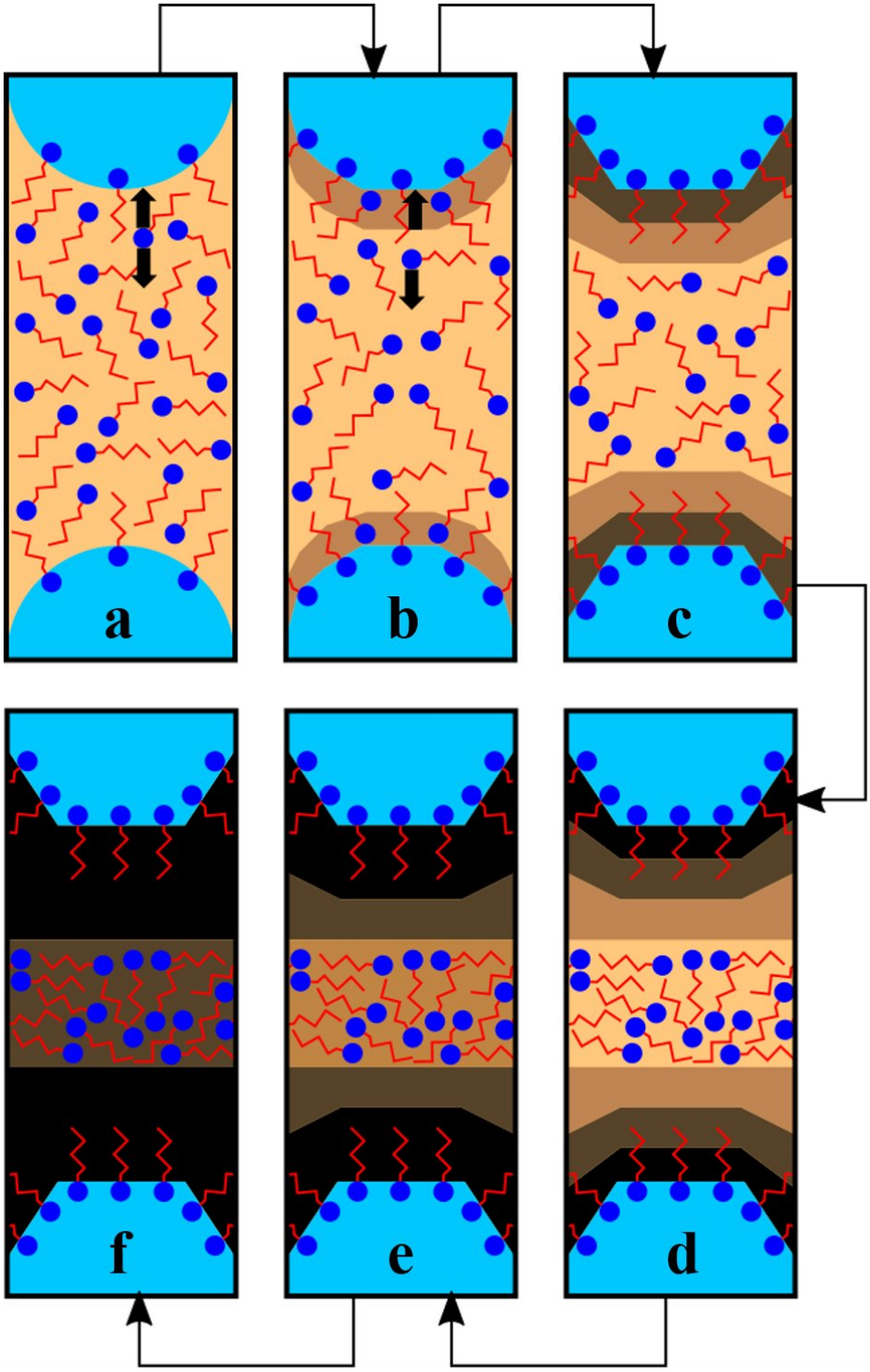

Figure 6: Schematic drawing of the mechanism that increases the area of the water/monomer interface and that creates non-porous outer layers and a porous inner layer in the pore wall.

On the one hand, the water/monomer interface is very close so that the surfactant molecules can diffuse to this interface (see Figure 6 (b, black arrow up)). As the surfactant molecules are not water-soluble, they remain at the water/monomer interface and overpopulate it with surfactant. The water/monomer interface, in turn, increases its area resulting in hexagonal pore

cross-sections (see Figure 6 (c and d)). When the polymerisation continues (see Figure 6 (c and d, light brown)), the regions close to the water/monomer interface will become more and more viscous and thus, any further surfactant diffusion will stop (see Figure 6 (c and d, black)). Diffusion towards the water/monomer interface is therefore only possible in the beginning of the polymerisation. Looking again at Figure 6 (b), one sees that the second option for the surfactant is to diffuse to the inside of the continuous monomer phase (see Figure 6 (b, black arrow down)). With the polymerisation continuing (see Figure 6 (c and d, brown to black)) the surfactant molecules are trapped and cannot move anywhere else anymore. The monomer molecules around them are eventually all polymerised which ultimately fixates the surfactant molecules (see Figure 6 (e and f)). The surfactant molecules stay at their location until they are washed out during purification resulting in the porous inner layer. Since all surfactant molecules have diffused away from the regions of the continuous monomer phase close to the water/monomer interface, no porosity is found in the outer layers.

5 Conclusion

The overall aim of this study was to identify the mechanism that explains the unexpected morphology of macroporous polymers when they are polymerised from monodisperse water-in-monomer HIPES with a water-soluble initiator. Firstly, the shape of the pores changes from spherical to polyhedral (hexagonal pore cross-sections) which means that the interfacial area increases during polymerisation. Secondly, the pore walls are layered with two outer layers and one inner layer. Varying the surfactant mass fraction of the HIPEs between 5 wt.% and 20 wt.%, one finds that the shape of the pore cross-sections does not change. At the same time, the relative area of the outer layer of the pore wall decreases, while the relative area of the inner layer increases with increasing the surfactant mass fraction. Thirdly, the outer layers are non-porous, while the inner layer is porous. In order to understand the answer of the surfactant to polymerisation, a model ternary phase diagram simulating the polymerization was used. It became clear that the surfactant wants to remain solubilized in the monomer and thus diffuses away from the polymerisation “zone” if possible. By combining all experimental results, a mechanism was derived that explains the morphology described above. When the polymerisation starts at the water/monomer interface, the surfactant becomes less and less soluble in the region close to the interface. In turn, the surfactant reacts by diffusing either to the water/monomer interface or to the continuous monomer phase. The first process leads to an overpopulation of the interface with surfactant and thus to an increase of interfacial area. As a

consequence, the pores deform from a spherical to a polyhedral shape and thus, hexagonal pore cross-sections are observed. The second process leads to an accumulation of surfactant inside the continuous monomer phase and a depletion of surfactant in the regions of the continuous monomer phase close to the interface. The final purification of the samples washes out the surfactant, which results in a porous inner and two non-porous outer layers. These conclusions are in contradiction to what was published previously [3], thus opening a new arena for the synthesis of macroporous polymers via emulsion templating. It is only with monodisperse systems that such a conceptually new analysis can be carried out. Using the traditional polydisperse templates for emulsion templating [16,17,19] one obtains macroporous polymers with a broad variety of pore sizes and wall thicknesses that do not allow analysing the origin of structural peculiarities. The only open question left is the enormous thickness of the pore walls. We speculate that the growing polymerisation zone exerts a pressure on the still liquid surfactant/monomer mixture. We also speculate that this pressure is larger in the struts than in the films. If this were the case, the liquid surfactant/monomer mixture would be pushed from the struts to the films. In order to answer this open question, we will carry out a time-resolved micro computed tomography (μ-CT) study.

Acknowledgement

We would like to thank the Institute for Combustion Technology from the University of Stuttgart for providing their SEM ("SEM1") and Prof. Dr. Alexander Fels for his help with the measurements. Furthermore, we would like to express our gratitude to Dr. Yaseen Qawasmi for recording the other SEM measurements ("SEM2"). For their help with recording and evaluating the SANS measurements, we would like to thank Apl. Prof. Dr. Thomas Sottmann, Karina Abitaev, Diana Zauser, Shih-Yu Tseng, and Julian Fischer. We are deeply thankful for the uncountable fruitful discussions with Dr. Wiebke Drenckhan.

Author Contributions

Lukas Koch: Conceptualization, Methodology, Investigation, Visualization, Writing – Orginal Draft; **Sophia Botsch:** Investigation; **Cosima Stubenrauch:** Conceptualization, Writing - Review & Editing, Supervision

References

[1] A. Quell, J. Elsing, W. Drenckhan, C. Stubenrauch, Monodisperse Polystyrene Foams via Microfluidics – A Novel Templating Route, Adv. Eng. Mater. 17 (2015) 604-609.

[2] A. Quell, B. de Bergolis, W. Drenckhan, C. Stubenrauch, How the Locus of Initiation Influences the Morphology and the Pore Connectivity of a Monodisperse Polymer Foam, Macromolecules 49 (2016) 5059-5067.

[3] A. Quell, S. Heitkam, W. Drenckhan, C. Stubenrauch, Creating Honeycomb Structures in Porous Polymers by Osmotic Transport, ChemPhysChem 18 (2017) 451-454.

[4] A. Quell, T. Sottmann, C. Stubenrauch, Diving into the Finestructure of Macroporous Polymer Foams Synthesized via Emulsion Templating: A Phase Diagram Study, Langmuir 33 (2017) 537-542.

[5] M. L. Dabrowski, D. Jenkins, E. Cosgriff-Hernandez, C. Stubenrauch, Methacrylate-based polymer foams with controllable connectivity, pore shape, pore size and polydispersity, Phys. Chem. Chem. Phys. 22 (2020) 155-168.

[6] H. Bartl, W. von Bonin, Über die Polymerisation in umgekehrter Emulsion, Macromol. Chem. Phys. 57 (1962) 74-95.

[7] J. M. Williams, D. A. Wrobleski, Spatial Distribution of the Phases in Water-in-Oil Emulsions. Open and Closed Microcellular Foams from Cross-Linked Polystyrene, Langmuir 4 (1988) 656-662.

[8] J. M. Williams, D. A. Wrobleski, Microstructures and properties of some microcellular foams, Journal of Materials Science Letters 24 (1989) 4062-4067.

[9] J. M. Williams, A. J. Gray, M. H. WilkersonEmulsion Stability and Rigid Foams from Styrene or Divinylbenzene Water-in-Oil Emulsions, Langmuir 6 (1990) 437-444.

[10] J. M. Williams, J. J. Bartos III, M. H. Wilkerson, Elastic modulus dependence on density for polymeric foams with systematic changing microstructures, Journal of Materials Science 25 (1990) 5134-5141.

[11] P. Hainey, I. M. Huxham, B. Rowatt, D. C. Sherrington, L. Tetley, Synthesis and Ultrastructural Studies of Styrene-Divinylbenzene Polyhipe Polymers, Macromolecules 24 (1991) 117-121.

[12] N. R. Cameron, D. C. Sherrington, L. Albiston, D. P. Gregory, Study of the formation of the open-cellular morphology of poly(styrene/divinylbenzene) polyHIPE materials by cryo-SEM, Colloid Polym. Sci. 274(6) (1996) 592-595.

[13] A. Barbetta, N. R. Cameron, S. J. Cooper, High internal phase emulsions (HIPEs) containing divinylbenzene and 4-vinylbenzyl chloride and the morphology of the resulting PolyHIPE materials, Chemical Communications 0 (2000) 221-222.

[14] H. Tai, A. Sergienko, M. S. Silverstein, Organic-inorganic networks in foams from high internal phase emulsion polymerizations, Polymer 42 (2001) 4473-4482.

[15] H. Tai, A. Sergienko, M. S. Silverstein, High Internal Phase Emulsion Foams: Copolymers and Interpenetrating Polymer Networks, Polymer Engineering and Science 41(9) (2001) 1540-1552.

[16] N. R. Cameron, High internal phase emulsion templating as a route to well-defined porous polymers, Polymer 46 (2005) 1439-1449.

[17] M. S. Silverstein, H. Tai, A. Sergienko, Y. Lumelsky, S. Pavlovsky, PolyHIPE: IPNs, hybrids, nanoscale porosity, silica monoliths and ICP-based sensors, Polymer 46 (2005) 6682-6694.

[18] A. Menner, R. Powell, A. Bismarck, A new route to carbon black filled polyHIPEs, Soft Matter 2 (2006) 337–342.

[19] S. D. Kimmins, N. R. Cameron, Functional Porous Polymers by Emulsion Templating: Recent Advances, Advanced Functional Materials 21 (2011) 211-225.

[20] M. S. Silverstein, PolyHIPEs: Recent advances in emulsion-templated porous polymers, Progress in Polymer Science 39 (2014) 199-234.

[21] R. S. Moglia, J. L. Holm, N. A. Sears, C. J. Wilson, D. M. Harrison, E. Cosgriff-Hernandez, Injectable PolyHIPE as High-Porosity Bone Grafts, Biomacromolecules 12 (2011) 3621-3628.

[22] R. S. Moglia, M. Whitely, P. Dhavalikar, J. Robinson, H. Pearce, M. Brooks, M. Stuebben, N. Cordner, E. Cosgriff-Hernandez, Injectable Polymerized High Internal Phase Emulsions with Rapid in Situ Curing, Biomacromolecules 15 (2014) 2870-2878.

[23] M. E. Whitely, J. L. Robinson, M. C. Stuebben, H. A. Pearce, M. A. P. McEnery, E. Cosgriff-Hernandez, Prevention of Oxygen Inhibition of PolyHIPE Radical Polymerization Using a Thiol-Based Cross-Linker, ACS Biomater. Sci. Eng. 3 (2017) 409-419.

[24] K.-Y. Chung, N. C. Mishra, C. C. Wang, F. H. Lin, K.-H. Lin, Fabricating scaffolds by microfluidics, Biomicrofluidics 3 (2009) 022403-(1-8).

[25] S.-W. Choi, I. W. Cheong, J. H. Kim, Y. Xia, Preparation of Uniform Microspheres Using a Simple Device and Their Crystallization into Close-Packed Lattices, Small 5(4) (2009) 454-459.

[26] J.-Y. Lin, W.-J. Lin, W.-H. Hong, W.-C. Hung, S. H. Nowotarski, S. Montenegro Gouveai, I. Cristo, K.-H. Lin, Morphology and organization of tissue cells in 3D microenvironment of monodisperse foam scaffolds, Soft Matter 7 (2011) 10010-10016.

[27] C.-C. Wang, K.-C. Yang, K.-H. Lin, H.-C. Liu, F.-H. Lin, A highly organized three-dimensional alginate scaffold for cartilage tissue engineering prepared by microfluidic technology, Biomaterials 32 (2011) 7118-7126.

[28] Y.-S. Sun, S.-W. Peng, K.-H. Lin, J.-Y. Cheng, Electrotaxis of lung cancer cells in ordered three-dimensional scaffolds, Biomicrofluidics 6 (2012) 014102-(1-14).

[29] C. Colosi, M. Costantini, A. Barbetta, R. Pecci, R. Bedini, M. Dentini, Morphological Comparison of PVA Scaffolds Obtained by Gas Foaming and Microfluidic Foaming Techniques, Langmuir 29 (2013) 82-91.

[30] G. Schwachula, Calculation of the copolymerization parameters in the ternary copolymerization system of styrene/m-divinyl-benzene/p-divinylbenzene, J. Polym. Sci.: Polymer Symposia 53 (1975) 107-112.

[31] L. Koch, W. Drenckhan, C. Stubenrauch, Porous polymers via emulsion templating: pore deformation during solidification cannot be explained by an osmotic transport!, ChemPhysChem (2020).

[32] N. Graeber, A Study of Fundamentals in Emulsion Templating for the Preparation of Macroporous Polymer Foams, PhD thesis (2013) p. 85 Imperial College London.

[33] A. M. Kraynik, D. A. Reinelt, F. van Swol, Structure of Random Foam, Phys. Rev. Lett. 93(20) (2004) 208301-(1-4).

[34] S. Hilgenfeldt, A. M. Kraynik, D. A. Reinelt, J. M. Sullivan, The structure of foam cells: Isotropic Plateau polyhedra, EPL 67(3) (2004) 484-490.

[35] A. M. Kraynik, D. A. Reinelt, F. van Swol, Structure of random bidisperse foam, Colloids and Surf. A 263 (2005) 11-17.

[36] A. M. Kraynik, The Structure of Random Foam, Adv. Eng. Mater. 8(9) (2006) 900-906.

[37] W. Drenckhan, S. Hutzler, Structure and energy of liquid foams, Adv. Colloid Interface Sci. 224 (2015) 1-15.

[38] T. Foster, T. Sottmann, R. Schweins, R. Strey, Small-angle neutron scattering from giantwater-in-oil microemulsion droplets. I. Ternary system, J. Chem. Phys. 128 (2008) 054502-(1-13).